ACADEMIC PRESS

Available online at www.sciencedirect.com

SCIENCE DIRECT®

Journal of Sound and Vibration 262 (2003) 907–919

JOURNAL OF SOUND AND VIBRATION

www.elsevier.com/locate/jsvi

Identification of a continuous structure with a geometrical non-linearity. Part II: Proper orthogonal decomposition

V. Lenaerts, G. Kerschen*, J.-C. Golinval

LTAS—Vibrations et Identification des Structures, Université de Liège, Chemin des Chevreuils 1 (B52), B-4000 Liège, Belgium

Received 12 October 2001; accepted 8 April 2002

Abstract

Particular effort has been spent in the field of identification of multi-degree-of-freedom non-linear systems. The newly developed methods permit the structural analyst to consider increasingly complex systems. The aim of this paper and a companion paper is to study, by means of two methods, a continuous non-linear system consisting of an experimental cantilever beam with a geometrical non-linearity. In the companion paper (Part I) [1] the ability of the conditioned reverse path method, which is a frequency domain technique, to identify the behaviour of this structure is assessed. This paper (Part II) is devoted to the application of proper orthogonal decomposition, which is an updating technique, to the test example.

1. Introduction

For the purpose of modelling, prediction and control of the dynamic behaviour of structures, modal testing and analysis are the most widely used linear techniques. However, when structures are subject to large displacement amplitudes, non-linear effects may become important and the linear model consequently fails. Even at low amplitudes, some non-linear distortions may occur due to dry friction for instance. Both reasons demonstrate why interest in non-linear identification is increasing.

As pointed out in Part I [1], the last twenty years have witnessed impressive progress in non-linear structural dynamics. Recently, the concept of a reverse path model, introduced by Bendat [2,3], has been extended to systems characterized by non-linearities away from the location of the applied force. This formulation, called the conditioned reverse path (CRP) method, allows

*Corresponding author. Fax: +32-4-366-48-56.

E-mail addresses: v.lenaerts@ulg.ac.be (V. Lenaerts), g.kerschen@ulg.ac.be (G. Kerschen).

0022-460X/03/$ - see front matter
doi:10.1016/S0022-460X(02)01132-X

conditioned frequency responses to be computed and yields the underlying linear properties without influence of non-linearities. The non-linear coefficients are identified in a second step.

New studies have now started to better take into account the spatial information. Adams and Allemang [4] have introduced a new principle of superposition for non-linear systems based on a spatial perspective of non-linearities as internal forces. Refs. [5,6] interpreted the proper orthogonal decomposition (POD) as a bi-orthogonal decomposition in space and time and also noticed some similarities between the POMs and the mode shapes.

The aim of this paper is to present a time domain method for the identification of non-linear parameters of a model. The proposed method investigates the use of spatial and time information contained in the POD to identify both linear and non-linear parameters of a dynamic structure.

2. Proper orthogonal decomposition

The POD, also known as Karhunen–Loeve (K–L) decomposition, is based on a statistical formulation, although it facilitates modal projections of partial differential equations into reduced-order deterministic models [7]. The K–L method was applied successfully in the fields of fluid dynamics [8], thermics [9] and signal processing [10].

The POD is a means of extracting spatial information from a set of time series available on a domain. The use of this transform is of great help in non-linear settings where traditional linear techniques such as modal testing and power spectrum analyses cannot be applied. The most striking property of the POD is its optimality in the sense that it minimizes the average squared distance between the original signal and its reduced representation.

It also allows spatial coherence in turbulence and structures to be quantified [11]. The application of POD to measured displacements of a discrete structure with a known mass matrix leads to an estimation of the normal modes [5,6]. In Ref. [7] the K–L method is applied to vibroimpacting beams and rotors to create low-dimensional models, via a Galerkin projection.

2.1. Mathematical formulation of the POD

The POMs are shown here to be the eigenfunctions of the space correlation tensor. Let us define a random field $y(x,t)$ on some domain Ω with zero-mean value. This field is sampled at a finite number of time points. Hence at a fixed time t_n, the system displays an instantaneous snapshot $y_n(x)$, which is a continuous function of x on Ω. Now a representative structure $\phi(x)$ of the ensemble of N snapshots is sought. This coherent structure is computed by minimizing the objective function λ:

$$\text{Minimize} \quad \left\{ \lambda = \sum_{n=1}^{N} (\phi(x) - y_n(x))^2 \right\} \quad \forall x \in \Omega. \tag{1}$$

Eq. (1) can be compactly expressed as the maximization problem:

$$\text{Maximize} \quad \left\{ \lambda = \frac{\langle (\phi, y_n)^2 \rangle}{(\phi, \phi)} \right\} \quad \forall x \in \Omega \tag{2}$$

with the following notations:

$$(f,g) \equiv \int_{\Omega} f(x)\, g(x)\, \mathrm{d}\Omega \quad \text{represents the inner product of } f \text{ and } g,$$

$$\langle y_n \rangle \equiv \frac{1}{N} \sum_{n=1}^{N} y_n(x) \quad \text{is the average of snapshots.}$$

This equation is equivalent to the following integral eigenvalue problem:

$$\int_{\Omega} K(x,x')\, \phi(x')\, \mathrm{d}x' = \lambda\, \phi(x'), \tag{3}$$

where the two-point correlation function $K(x,x')$ is defined as

$$K(x,x') = \frac{1}{N} \sum_{n=1}^{N} y_n(x)\, y_n(x'). \tag{4}$$

Eq. (3) has a finite number of orthogonal solutions $\phi^i(x)$ with corresponding real and positive eigenvalues λ^i. The eigenvalue with the largest magnitude is the maximum which is achieved in the maximization problem (2). The second largest eigenvalue is the maximum of the same problem restricted to the space orthogonal to the first eigenfunction, and so on. In order to make the computation unique, the eigenfunctions are normalized. Therefore it can be used as a basis for the decomposition of the field

$$y(x,t) = \sum_{i=1}^{N} a^i(t)\, \phi^i(x). \tag{5}$$

Moreover, by construction, the POMs capture more energy than any other modes. It should also be noted that time-dependent coefficients $a^i(t)$ in Eq. (5) are uncorrelated [12]. As can be seen from Eq. (5), POD may thus be viewed as a bi-orthogonal decomposition because of the space–time symmetry of the decomposition. It allows the identification of a useful set of basic functions and the dimension of the subspace necessary to achieve a satisfactory approximation of the system. The POD also facilitates the resolution of the partial differential equations through their projection into a reduced-order model [7,13].

2.2. Discrete formulation

Suppose that N linear snapshots $\mathbf{y}_i$ of size M are obtained at M locations (e.g., by use of accelerometers):

$$\mathbf{y}_i = [y(x_1,t_i), \quad \ldots \quad , y(x_M,t_i)], \quad i = 1, \ldots, N. \tag{6}$$

The $M \times M$ covariance matrix $\mathbf{C}$ [10] is defined as

$$\mathbf{C} = \frac{1}{N} \sum_{i=0}^{N-1} \mathbf{y}_i \mathbf{y}_i^{\mathrm{T}}. \tag{7}$$

Its eigensolutions (ϕ_k, λ_k) which satisfy

$$\mathbf{C}\phi_k = \lambda_k \phi_k, \quad k = 0, \ldots, N-1 \tag{8}$$

with

$$\lambda_0 \geqslant \lambda_1 \geqslant \cdots \geqslant \lambda_{N-1} > 0 \tag{9}$$

correspond to the POD of the system. If the eigenvalues are normalized, they represent the relative energy captured by the corresponding POM. This decomposition is the best basis in terms of de-correlation.

2.3. Computation of the POD using singular value decomposition

The complete bi-orthogonal decomposition of the data may be obtained by use of singular value decomposition (SVD). Let the discrete matrix:

$$\mathbf{Y} = \begin{bmatrix} y(x_1, t_1) & \cdots & y(x_1, t_N) \\ \vdots & \ddots & \vdots \\ y(x_M, t_1) & \cdots & y(x_M, t_N) \end{bmatrix}, \tag{10}$$

where each row corresponds to a time history at one location and each column corresponds to a snapshot of the system at a specific time. The SVD of matrix $\mathbf{Y}$ can be written as

$$\mathbf{Y} = \mathbf{U}\boldsymbol{\Sigma}\mathbf{V}^{\mathrm{T}} \tag{11}$$

with $\mathbf{U}$ an orthonormal matrix (size $M \times M$) containing the eigenvectors of $\mathbf{Y}\mathbf{Y}^{\mathrm{T}}$ and $\mathbf{V}$ an orthonormal matrix (size $N \times N$) containing the eigenvectors of $\mathbf{Y}^{\mathrm{T}}\mathbf{Y}$. The size of the matrix $\boldsymbol{\Sigma}$ is $M \times N$ but only the main diagonal has non-zero elements which are the singular values of $\mathbf{Y}$, sorted in descending order.

From the definition of the SVD, it follows that each column of $\mathbf{U}$ corresponds to a POM $\boldsymbol{\phi}_k$ while each line of $\mathbf{V}$ contains the time coefficients of the corresponding POM.

Note also that SVD is used in Refs. [14,15] to compute modal metrics to solve model updating problems using an optimization procedure.

3. Application to parameter identification

In our approach, the identification of the non-linear parameters of a structure is formulated in terms of an optimization problem which consists of minimizing the difference between the bi-orthogonal decompositions of the measured and simulated data, respectively. The objective function F is defined as

$$F = \sum_i \sum_j (\Delta U_{ij})^2 + \sum_j (\Delta \Sigma_{jj})^2 + \sum_j \sum_k (\Delta V_{jk})^2, \tag{12}$$

where ΔU_{ij}, $\Delta \Sigma_{jj}$ and ΔV_{jk} are the differences between the matrices containing the bi-orthogonal decompositions, i.e., the differences between the SVD of the measured and simulated data (Eq. (11)). It should be noted that the full decomposition is not retained in the objective function. Only the terms corresponding to the highest singular values are considered (see Ref. [16] for more details), which means that only the POMs that contain the greatest amount of energy in the signal are considered.

In order to retain the time information but without the drawback of its oscillatory nature, the wavelet transform or the windowed discrete-time Fourier transform of the time decomposition associated with each POM is computed. This gives a time–frequency representation of the energy contained in the signal. The instantaneous frequencies of the signal that correspond to the maximum of the transform are extracted. This information, which is time dependent, as well as the envelope corresponding to these maxima, are included in the objective function (12) instead of the right-singular vectors. It allows smoothing of the objective function as it transforms the oscillatory nature of the time information into a more suitable one [16]. The objective function F may then be minimized using standard optimization algorithms.

4. Analysis results: horizontal set-up

The description of the set-up can be found in Part I of this work [1]. Seven accelerometers which span the beam regularly are used to measure the response, but in this case the structure is excited with a hammer at co-ordinate number 6.

4.1. F.E. model of the structure

The main steel beam is modelled with seven beam finite elements and the thin part with four beam finite elements (Fig. 1). An additional element is used to model the junction between the two beams. This element connects the rotational and translational degree-of-freedom of the main and thin beams by rotational and translational stiffnesses. Prior to the non-linear analysis, an updating of the model considered as linear was performed at very low level of excitation. For this purpose, the rotational and translational stiffnesses at the two clamped ends and at the junction were chosen as updating parameters.

4.2. Identification of the non-linear parameters

Based on the results obtained in Part I, the non-linear behaviour of the system is modelled by grounded quadratic and cubic springs at the junction:

$$f(x) = A|x|^3\mathrm{sign}(x) + B|x|^2. \tag{13}$$

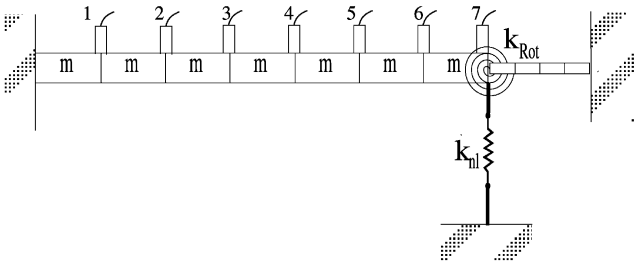

Fig. 1. Model of the structure.

The cubic term takes the stiffening effect of the thin part into account while the quadratic term is related to the presence of the second harmonic of the first mode in the measured data.

The choice of the damping model is a major issue to predict the free response of the system. A modal damping model is still considered but obviously, is not the same as for the linear case. Indeed, large displacements tend to induce more damping in the system. The parameters to identify in the non-linear case are thus the cubic and quadratic stiffnesses as well as the damping ratio of the first four modes of the underlying linear system.

The time response of the system was computed over a time period of 2.34 s with a sampling frequency of 2560 Hz. The instantaneous frequencies and envelopes corresponding to the time decomposition $\mathbf{V}$, the POMs contained in $\mathbf{U}$, and Σ values (see Eq. (11)) for both simulated and experimental cases are introduced in the objective function (12). The objective function is written in terms of the first four POMs which represents 99% of the total energy of the signal. The optimization process then yields the solution of the parameter identification.

After updating, the values of the quadratic and cubic stiffnesses are respectively 7.9×10^6 N m^{-2} and 6.1×10^9 N m^{-3}, which is of the same order of magnitude than the values found using the CRP method in Part I.

The instantaneous frequency and envelope corresponding to the maxima on the time–frequency plane of the time decomposition are plotted in Fig. 2 (first POM). The reconstructed instantaneous frequency and envelope for this POM match the experimental ones with a maximal relative error of 8%. This may be substantially improved. As already pointed out in Part I, the problem comes from the second harmonic which is due to gravity. It indicates that the model is not suited in this case to represent the system well.

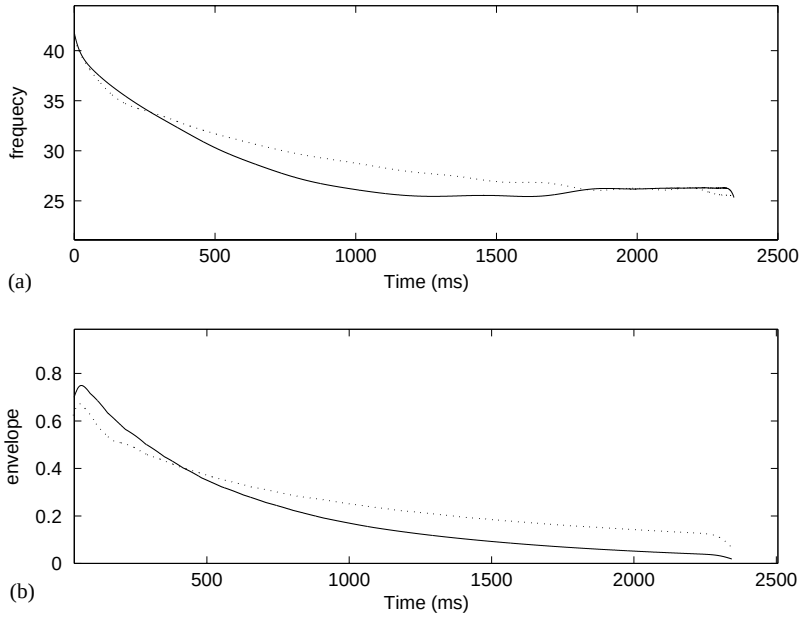

Fig. 2. Time–frequency properties of the first POM (horizontal set-up). ———, Experimental system; ···, updated non-linear model. (a) Instantaneous frequency; (b) envelope.

5. Analysis results: vertical set-up

As pointed out in Part I, the vertical set-up was built to reduce the asymmetrical influence of gravity. In this section, the POD is again exploited to identify the non-linear behaviour of the thin part.

5.1. Updating of the linear part

As the horizontal set-up was completely dismounted and rebuilt in a vertical position, a new updating of the model considered as linear was performed. It allowed possible discrepancies in the linear model due to mounting/dismounting purposes to be eliminated.

5.2. Identification of the non-linear parameters

As in Section 4.2, the thin beam part is modelled using a grounded symmetrical non-linearity but since the effect of gravity is now negligible, the asymmetrical non-linearity may be discarded from the model, i.e.,

$$f(x) = A|x|^{\alpha}\mathrm{sign}(x). \tag{14}$$

The parameters to identify are coefficients A and α as well as the damping ratio of the first four modes for the underlying linear system.

The time response of the system was computed over a time period of 1.34 s with a sampling frequency of 5120 Hz. Different initial values of parameters for the optimization have been tested to avoid local minima. Of course there is no guarantee to obtain the global minimum by classical optimization methods but the starting point has been chosen close to the assumed solution. For example the initial cubic stiffness can be chosen according to the instantaneous frequency of the first POM at the beginning of the measurements. After updating, the best results in terms of the objective function are a non-linear exponent $\alpha = 2.8$ and a non-linear coefficient $A = 1.65 \times 10^9\ \mathrm{N/m^{2.8}}$.

Fig. 3 shows the comparison between the first four reconstructed POMs of the linear updated model of the structure, the experimental POMs and the reconstructed POMs of the non-linear model, excited by the same measured impulsion. From these figures, it can be observed that the non-linearity mainly acts on the first and second POMs. After updating, the first and second POMs of the non-linear model closely match the experimental ones.

Fig. 4 compares the time–frequency characteristics of the time decomposition of the first POM for the different models. Plots (a1) and (a2) are respectively the PSD and the windowed discrete-time Fourier transform corresponding to the experimental data. Plots (b1) and (b2) correspond to the updated non-linear model while plots (c1) and (c2) correspond to the underlying linear model. As expected, the linear model clearly exhibits a PSD with two thin peaks at the first two eigenfrequencies and the corresponding energy on the time–frequency plane concentrates around this two frequencies with no decrease in time. The PSD corresponding to the experimental data and to the non-linear model show larger peaks around this two frequencies. The energy in the time–frequency plane concentrates around different characteristic frequencies such as the frequencies of the underlying linear structure (i.e., 30, 142 and 393 Hz) and the different

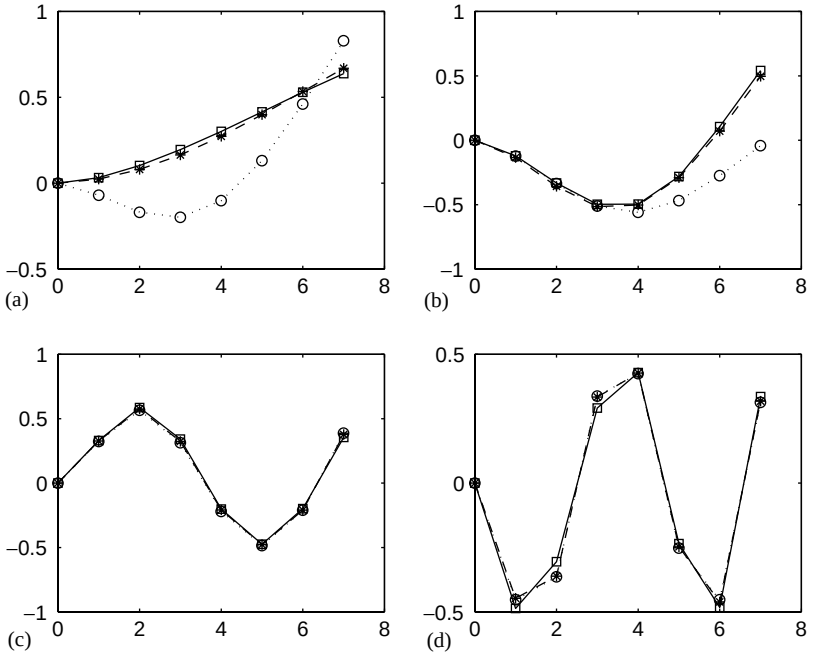

Fig. 3. POMs (vertical set-up). ——□——, Experimental POM; ⋯○⋯, linear model; — ∗ —, updated non-linear model. (a) First POM; (b) second POM; (c) third POM; (d) fourth POM.

harmonics or their combinations, i.e., the third harmonic of the first resonance around 110 Hz. These particular frequencies also appear in the PSD plot while they are not present for the linear model.

In Fig. 5, the instantaneous frequency and envelope corresponding to the maxima in the time–frequency plane of the first POM time decomposition are plotted for the different models. It can be seen that the instantaneous frequency of the non-linear model matches the experimental one and clearly decreases in time to reach the natural frequency of the underlying linear system. This is expected of course since the amplitude of the vibration decreases in time and consequently, the stiffening effect of the non-linearity becomes less important.

Figs. 6 and 8 compare the time–frequency characteristics of the time decomposition of second and third POMs for the different models while Figs. 7 and 9 show the comparison of the corresponding instantaneous frequencies. The same behaviour as for the first POM can be observed but it is worth pointing out that the energy in the time–frequency planes concentrates more around the second and third resonance for the second and third POM respectively. Again the corresponding instantaneous frequencies decrease respectively to the second and third natural frequencies of the underlying linear system.

The maximum relative error on the instantaneous frequencies of the first three POMs is about 2%. The comparison between Figs. 5 and 2 indicates that the reconstructed instantaneous frequency of the first POM is a better match for the horizontal set-up than for the vertical set-up, despite a simpler non-linear model. This confirms the fact that gravity has a significant influence on the results for the horizontal set-up.

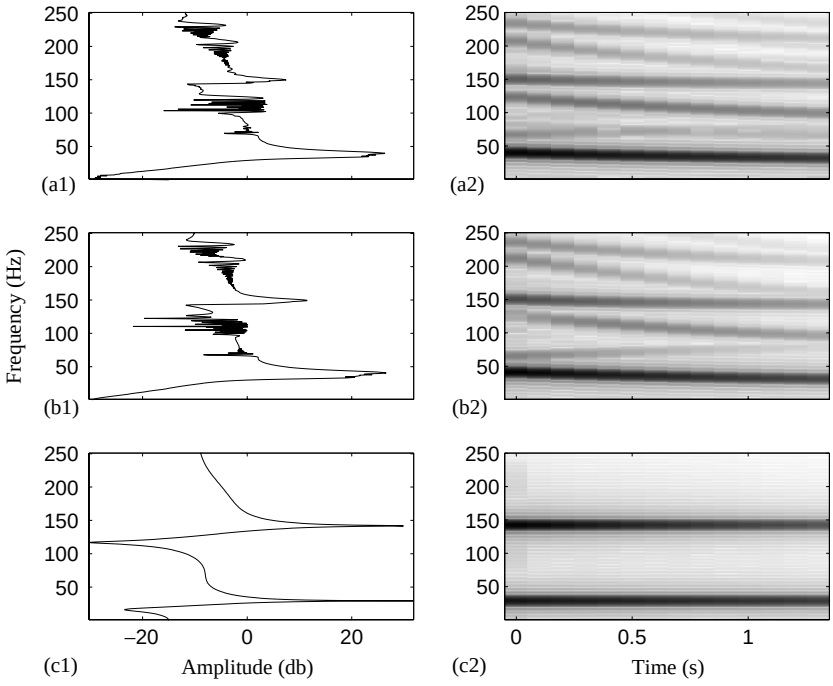

Fig. 4. Time–frequency properties of the first POM (vertical set-up). (a) Experimental system; (b) non-linear updated model; (c) linear updated model; (1) PSD of the time decomposition; (2) windowed discrete-time Fourier transform of the time decomposition.

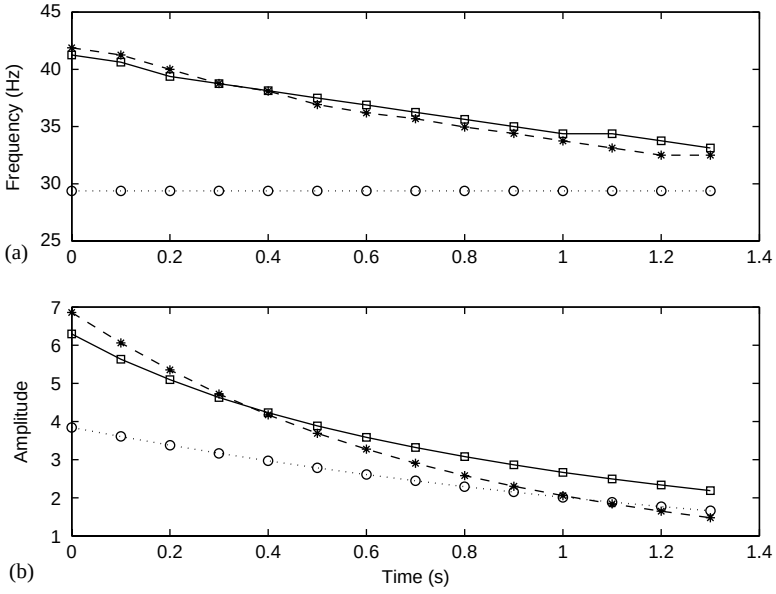

Fig. 5. Time–frequency properties of the first POM (vertical set-up). ——□——, Experimental system; ··· ○ ···, linear model; — ∗ —, updated non-linear model. (a) Instantaneous frequency; (b) envelope.

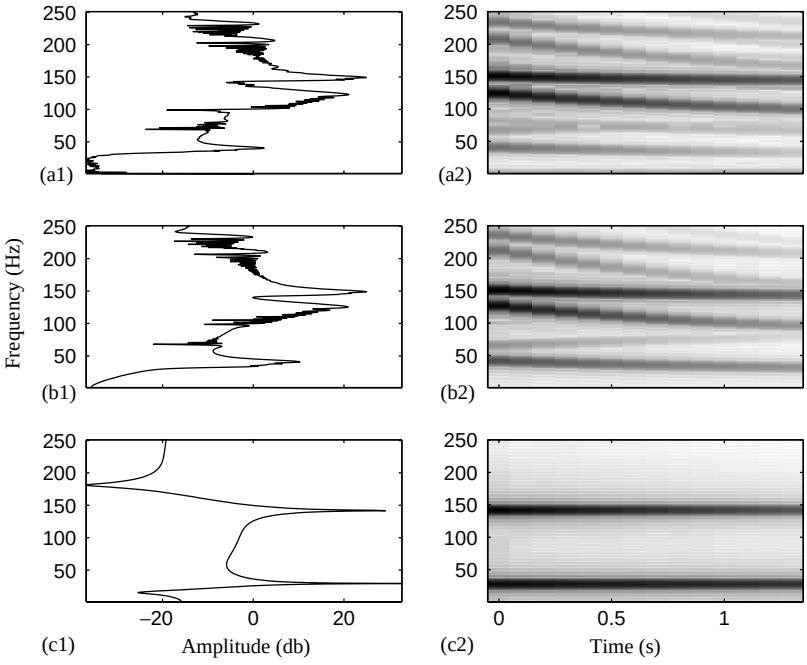

Fig. 6. Time–frequency properties of the second POM (vertical set-up). (a) Experimental system; (b) non-linear updated model; (c) linear updated model; (1) PSD of the time decomposition; (2) windowed discrete-time Fourier transform of the time decomposition.

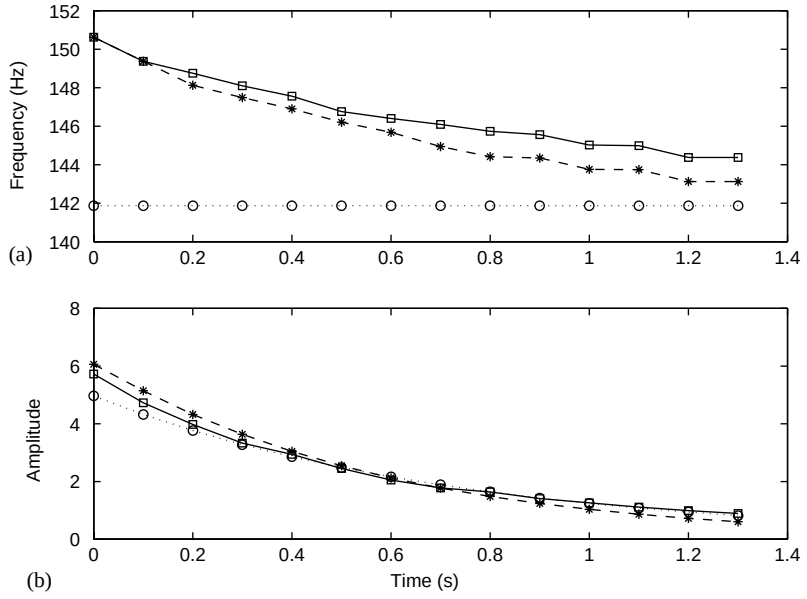

Fig. 7. Time–frequency properties of the second POM (vertical set-up). ——□——, Experimental system; ⋯○⋯, linear model; — ∗ —, updated non-linear model. (a) Instantaneous frequency; (b) envelope.

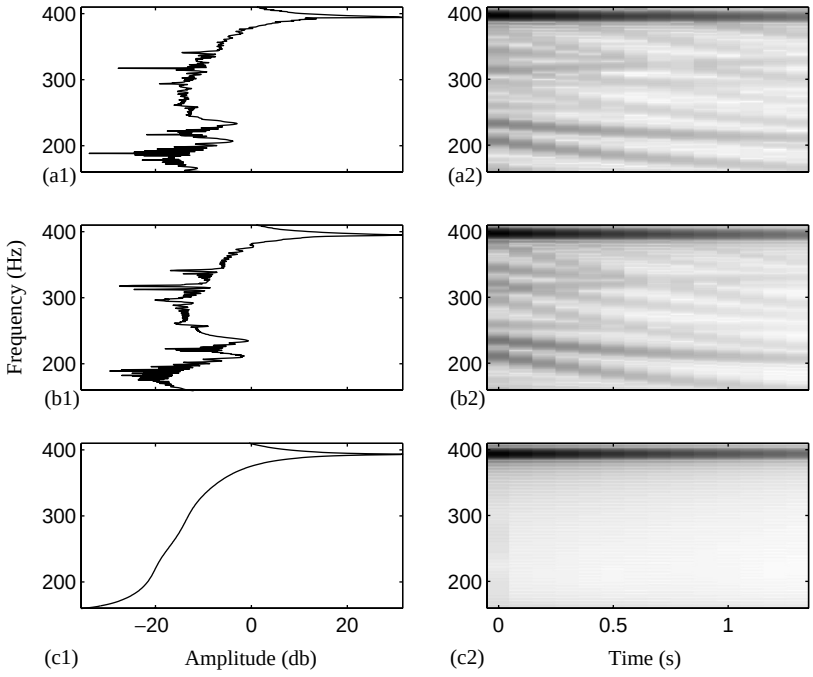

Fig. 8. Time-frequency properties of the third POM (vertical set-up). (a) Experimental system; (b) non-linear updated model; (c) linear updated model; (1) PSD of the time decomposition; (2) windowed discrete-time Fourier transform of the time decomposition.

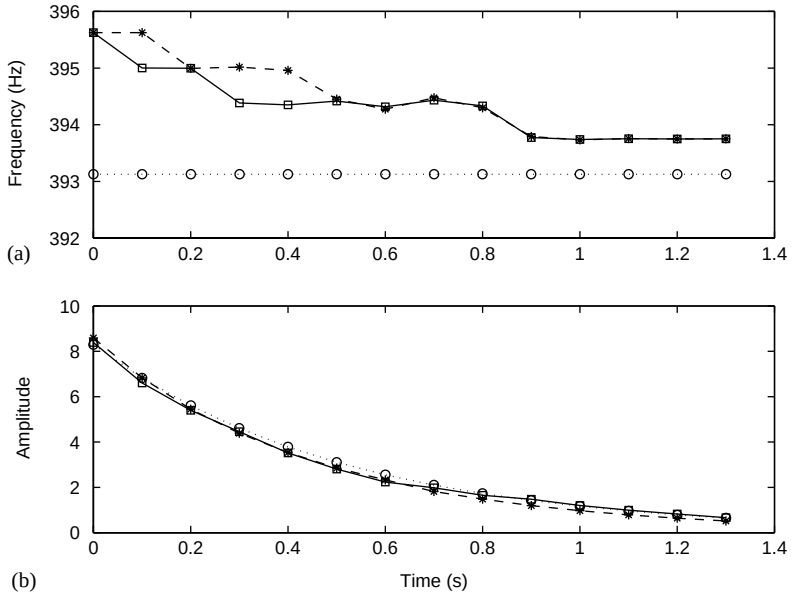

Fig. 9. Time–frequency properties of the third POM (vertical set-up). ——□——, Experimental system; ⋯○⋯, linear model; — ∗ —, updated non-linear model. (a) Instantaneous frequency; (b) envelope.

6. Comparison of the methods and conclusions

Although the CRP and the POD methods are different, similar results were obtained on the set-up considered in this work:

- having specified the same functional form of the non-linearity for both methods, the same kind of non-linearity has been identified, i.e., a $|x|^{2.8}\text{sign}(x)$ non-linearity;
- the non-linear coefficient identified with the POD method is slightly lower than the coefficient obtained with the CRP method for the highest level of excitation, i.e., 1.65×10^9 versus 1.96×10^9 N/m$^{2.8}$. This difference may be due to the different means of excitation used in both methods (hammer impact for POD and shaker for CRP).

Both methods are appealing because of their ability to consider multi-degree-of-freedom non-linear systems. The key advantage of POD is that the non-linear coefficients as well as structural matrices are obtained through the updating procedure. The CRP formulation only identifies the non-linear coefficients and the modal parameters of the underlying linear system rather than a physical model of the structure. Besides, the CRP method does not require any a priori knowledge of the structure (e.g., proportional damping assumption) while this knowledge is necessary in all updating processes. This feature allows the exploitation of the CRP technique to characterize the non-linearity prior to the identification. The methods are then complementary in the sense that the results given by the CRP method may be exploited as an initial point for the optimization procedure in the POD method.

The interest of the POD and CRP methods compared to other identification techniques lies in their ability to deal with continuous multi-degree-of-freedom systems. In this context, the results presented here are promising regarding to the difficult challenge of non-linear system identification in structural dynamics.

Acknowledgements

Mr. Kerschen is supported by a grant from the Belgian National Fund for Scientific Research (FNRS) which is gratefully acknowledged.

References

[1] G. Kerschen, V. Lenaerts, J.-C. Golinval, Identification of a continuous structure with a geometrical non-linearity. Part I: Conditioned reverse path method, Journal of Sound and Vibration, this issue.
[2] J.S. Bendat, Nonlinear System Analysis and Identification from Random Data, Wiley, New York, 1990.
[3] J.S. Bendat, Spectral techniques for nonlinear system analysis and identification, Shock and Vibration 1 (1993) 21–31.
[4] D.E. Adams, R.J. Allemang, Characterisation of nonlinear vibrating systems using internal feedback and frequency response modulation, American Society of Mechanical Engineers Journal of Vibration and Acoustics 121 (1999) 495–500.
[5] B.F. Feeny, Interpreting proper orthogonal modes in vibrations, Proceedings of DET'97 Design Engineering Technical Conferences, Sacramento, USA, 1997.

[6] G. Kerschen, J.C. Golinval, Physical interpretation of the proper orthogonal modes using the singular value decomposition, Journal of Sound and Vibration 249 (5) (2002) 849–865.
[7] M.F.A. Azeez, A.F. Vakakis, Numerical and experimental analysis of the nonlinear dynamics due to impacts of a continuous overhung rotor, Proceedings of DETC'97, ASME Design Engineering Technical Conferences, Sacramento, USA, 1997.
[8] J.L. Lumley, The structure of inhomogeneous turbulent flows, in: A.M. Yaglom, V.I. Tatarski (Eds.), Atmospheric Turbulence and Radio Wave Propagation, Nauka, Moscow, 1967.
[9] A. Newman, P.S. Krishnaprasad, Non-linear Model Reduction for RTCVD, Proceedings of the 32nd Conference on Information Sciences and Systems, Princeton, USA, 1998.
[10] G. Uytterhoeven, Software and Applications, Ph.D. Thesis, Katholieke Universiteit Leuven, 1999.
[11] J.P. Cusumano, B.-Y. Bai, Period-infinity periodic motions, chaos, and spatial coherence in a 10 degree of freedom impact oscillator, Chaos Solitons Fractals 3 (1994) 515–536.
[12] W. Casemier, Proper Orthogonal Decomposition and Low Dimensional Models for Turbulent Flows, Ph.D. Thesis, Rijksuniversiteit Groningen, 1997.
[13] M.F.A. Azeez, A.F. Vakakis, Proper orthogonal decomposition (POD) of a class of vibroimpact oscillations, Internal report, Department of Mechanical and Industrial Engineering, University of Illinois at Urbana Champaign, 1998.
[14] F.M. Hemez, S.W. Doebling, Test analysis correlation and finite element model updating for nonlinear transient dynamics, Proceedings of the 17th International Modal Analysis Conference, Kissimmee, USA, 1999, pp. 1501–1510.
[15] T.K. Hasselman, M.C. Anderson, W.G. Gan, Principal component analysis for nonlinear model correlation, updating and uncertainty evaluation, Proceedings of the 16th International Modal Analysis Conference, Santa Barbara, USA, 1998, pp. 644–651.
[16] V. Lenaerts, G. Kerschen, J.-C. Golinval, Proper orthogonal decomposition for model updating of non-linear mechanical systems, Mechanical Systems and Signal Processing 15 (1) (2001) 31–43.